Fluxgate three-component magnetometers for cost-effective ground, UAV and airborne magnetic surveys for industrial and academic geoscience applications and comparison with current industrial standards through case studies

Bruno Gavazzi, Pauline Le Maire, Jeanne Mercier de Lepinay, Paul Calou, Marc Munschy

HAL Id: hal-02446707
https://hal.science/hal-02446707

Submitted on 1 Feb 2021

1 **Fluxgate three-component magnetometers for cost-effective ground, UAV and airborne magnetic**

2 **surveys for industrial and academic geoscience applications and comparison with current industrial**

3 **standards through case studies**

4 Gavazzi B. (corresponding author)[1], Le Maire P.[1,2], Mercier de Lépinay J.[1], Calou P.[1,3], Munschy M.[1]

5

6 [1] Institut de Physique du Globe de Strasbourg, Ecole et Observatoire des Sciences de la Terre,

7 Université de Strasbourg et CNRS (IPGS UMR71516), Strasbourg, France.

8 [2] CARDEM/EUROVIA, Bischeim, France.

9 [3] ECA-EN, Groupe ECA, Coueron, France.

10 bgavazzi@unistra.fr ; Phone +33368850473 ; mobile +33607639713 ; address: IPGS, 1 rue Blessig,

11 67084 Strasbourg Cedex, France

12

13 **Abstract**

14 In applied geophysics, magnetic methods are used in a wide range of industrial and academic

15 applications with environmental, engineering or exploration components (e.g. military ordnance

16 detection, pipe detection, archaeology, resources exploration, geological mapping). According to the

17 type of application and the scale of the study, surveys can be conducted on the ground or airborne,

18 each having its own industrial standard. In ground survey applications single component or scalar

19 gradiometers are widely used. In airborne surveys the intensity of the magnetic field is measured

20 with scalar magnetometers and the disturbances of the aircraft are compensated with real-time

21 compensation unit.

22 This paper proposes another approach using the latest developments on the use of fluxgate three-

23 component magnetometers. They have a light weight, a low power consumption, are rugged and

24 allow a simple magnetic compensation of the carrier. They can provide a more precise and/or a more

25 cost effective alternative to current measuring standards. They can also be mounted on UAVs to fill

26 the gap in measurement capabilities between ground and airborne surveys, and therefore offer a

27 new range of applications. A review of four case studies concerning archaeology, unexploded

28 ordnance detection, lithology and structural geology studies is presented to illustrate the possibilities

29 of application of such an approach and how it compares to current industrial standards in ground and

30 airborne surveys.

1. Introduction

Applied Geophysics can be defined as the science of measurement and interpretation of physical properties to study sub-surface conditions. It plays therefore an important role in economic activities and academic research dealing with solid earth, from surface to the core, by providing non-intrusive and large scale data for imaging the underground. Practical applications are numerous[1], such as archaeology, engineering, environmental studies, mineral prospecting or hydrocarbon, geothermal and groundwater exploration. Different kind of methods exist, each based on a particular physical property. Geomagnetic methods consist in the measurement, processing and interpretation of spatial variations in the earth magnetic field linked to heterogeneities of the underground. They are passive methods, i.e. they are not based on reactions to external stimuli but on naturally occurring phenomena. They can be used in all the applications cited above, either in combination with other methods, or alone[1,2,3,4]. This vast range of potential applications led to the development of different methods and strategies for measuring the magnetic field depending on the scale and object of study: scalar or vector, gradient or total field, ground or airborne. However, the latest results on the use of vector magnetometers offer new possibilities for cost efficient and well compensated magnetic data acquisition on the ground, UAVs or aircrafts[5]. This paper aims to explore the industrial and scientific potentials of such possibilities through a discussion on the theory and current industrial standards, an explanation on how to use fluxgate three-component magnetometers for surveying and a review of case studies for different applications.

2. Main principles of geomagnetic methods and measuring standards

2.1 Main principles

Magnetism is a natural phenomenon resulting from movements of electrical charges at the atom level. These movements can be permanent (remanent magnetization) or a reaction to an external magnetic field (induced magnetization). At the macroscopic scale, materials can be characterized by their magnetization defined by a direction and an intensity in $A.m^{-1}$. Such magnetization is a sum of a remanent and an induced part. The remanent part is linked to the composition and formation processes of the material, while the induced part is also linked to the main geomagnetic field generated by deep internal sources (mainly the earth core). This main geomagnetic field varies in direction and intensity (from 20 000 to 70 000 nT on the surface) according to the position on the globe (mainly the latitude). Thus the magnetization of materials and associated magnetic fields are dependent on their composition as well as their geographical coordinates.

The basic principle of geomagnetic methods is to measure the magnetic field above the surface. This total magnetic field is a combination of the effect of all the sources, deep and superficial. Therefore,

64   heterogeneities of materials within the ground are generating spatial variations of the magnetic field

65   above the surface, usually in the range of a few nT to a several 1000 nT in applied geophysical

66   applications[6,7]. All geomagnetic methods consist in the quantification of such spatial variations, called

67   anomalies, in the earth magnetic field. For each measurement, the magnetic anomaly can be defined

68   as

$$\vec{A} = \vec{B} - \vec{R}, \tag{1}$$

69   where $\vec{A}$, $\vec{B}$ and $\vec{R}$ are the magnetic anomaly field, the measured total magnetic field and the main

70   (or regional) geomagnetic field respectively. $\vec{R}$ is given by the International Geomagnetic Reference

71   Field (IGRF) which is a model of the geomagnetic field based on data from surveys, magnetic

72   observatories and satellites[8]. Due to technical limitations, only the intensity of the total magnetic

73   field can be measured in motion accurately enough for applied geophysical applications. Therefore,

74   the anomaly of the intensity, or total field anomaly, noted C, is defined as

$$C = \|\vec{B}\| - \|\vec{R}\|. \tag{2}$$

75   As $\|\vec{B}\| = \|\vec{A} + \vec{R}\|$ and $\|\vec{A}\| \ll \|\vec{R}\|$, equation (2) can also be written:

$$C \approx \|\vec{A}\| \cos \alpha, \tag{3}$$

76   where α is the angle between $\vec{A}$ and $\vec{R}$. Thus the total field anomaly C is approximately equal to the

77   component of $\vec{A}$ in the direction of $\vec{R}$. This means that if $\vec{R}$ can be considered as a constant, which is

78   the case at scales used in applied geophysics, the total field anomaly C is a potential that satisfies

79   Laplace's equation, i.e. it allows the use of potential field theory for interpretation.

80   2.2 Industrial measuring standards

81   Regardless of the measuring method, the main issues to obtain exploitable measurements are the

82   reduction of the impact of natural and anthropogenic time-dependent variations (temporal

83   correction) as well as the reduction of the impact of the magnetizations of the measuring device or

84   carrier itself on the sensor (magnetic compensation). In addition, positioning should be managed

85   carefully, as imprecision in positioning or too sudden variation of acceleration of the moving

86   measuring device can lead to noise. Positioning systems offering 1 to 10 cm precision at 1 to 10 Hz

87   are usually used. Natural time-dependent variations are linked to the sun activity and its interaction

88   with earth. They consist of cycles of different periods (6 hours to tenths of years) with a daily

89   variation that usually does not exceed 100 nT, as well as unpredictable magnetic storms with

90   variations ranging up to a few hundred nT during a few hours to a few days. Anthropogenic variations

91   are more local. They can be due to electromagnetic fields (e.g. generated by power lines) or metallic

92   masses in movement near the measurements (e.g vehicles). Their frequencies are usually higher than

93   the hertz and with various intensities that can reach up to more than 10 000 nT. Variations due to the

94   magnetizations of the device and carrier are dependent on the distance between magnetometers

95   and the other components of the device as well as the composition, orientation and speed of the

96   carrier. For example, a plane in a typical airborne survey can cause variations of 500-1000 nT with a

97   standard deviation of more than 100 nT.

98   To address all these issues, different types of magnetometers or measuring strategies are used:

99   - For airborne surveys, the industrial standard is to use optically pumped alkali vapor (usually cesium)

100 scalar magnetometers. They have a sensitivity of around 0.1 nT and can make measurements at a

101 maximum frequency of 10 Hz. The temporal correction is evaluated from the data of a base station

102 placed on the field or of a near magnetic observatory. The magnetic compensation is carried out with

103 an automatic aeromagnetic digital compensation system (AADC) generating in real time a magnetic

104 field opposed to the one of the aircraft according to its position and orientation[9,10]. The parameters

105 of such a correction field are assessed and controlled for each survey through control flights in four

106 directions (N, E, S, W) with pitch, roll and yaw movements. The residual error after correction during

107 this maneuver should not excess 2 nT[10]. Parallel magnetic profiles are flown with a ratio

108 height/spacing usually between 1:1 to 1:2.5. The height of the flight is fixed accordingly to the level

109 of details required, usually between 50 and 500 m. Tie lines perpendicular to the profiles are also

110 flown with a greater spacing. The differences at the crossing points between profiles and tie lines

111 after all processing allow to assess the overall quality of the dataset, as it takes into account all

112 sources of noise, such as positioning errors, uncompensated magnetizations or uncorrected time-

113 dependent variations. The overall quality criterion depends on the study but is usually set under a

114 few nT.

115 - For ground survey, industrial standards are less strict. The temporal correction is performed either

116 with the use of a base station, as in aeromagnetic surveys, or by using a gradiometer for the survey:

117 the difference in signal is recorded between two sensors placed at a fixed distance in any direction

118 (often vertically). Thus the time-dependent variations can be considered the same on the two

119 sensors and therefore do not influence the measurements. The compensation is usually not

120 computed but the magnetometers are shifted from the rest of the equipment to reduce its impact.

121 The most used devices are by far vector gradiometer (single-component fluxgates), but scalar

122 gradiometers (alkali vapor or precession) and scalar magnetometers (alkali vapor or precession) are

123 also used[3,11,12,13]. Sensors are usually positioned between 0.5 and 1 m above the ground. Parallel

124 profiles are measured with a height/spacing ratio between 2:1 and 1:1 with both values between

125 0.25 and 1 m. Multi-sensor devices, especially vector gradiometers, are used to measure different

126 profiles simultaneously and therefore increase surveying speed. They usually consist of 2 to 5

127 gradiometers that can be carried, pushed on a cart or pulled behind a vehicle. In contrast with

128 airborne surveys, the overall quality of a dataset is usually difficult to assess as most of the time no

129 quality control procedure, such as tie-line, is planned.

130 2.3 Signal processing and interpretation.

131 Different parameters have to be taken into consideration for interpretation of the magnetic data.

132 The shape of the anomaly created by a magnetic source depends on the source 's magnetic and

133 geometric properties, the distance between source and sensor as well as the properties of the

134 regional magnetic field at the location which are mostly linked to its latitude . This can be illustrated

135 through a synthetic case with buried structures of different magnetizations and shapes placed at

136 different depths (Figure 1). The magnetic field of such structures can be computed from a

137 distribution of simpler spherical sources of a radius a. The magnetic field $\vec{A}(x, y, z)$ of such source

138 centered in $Q(x', y', z')$ at the observation point $P(x, y, z)$ is expressed as[6]

$$\vec{A}(x, y, z) = \frac{\mu_0}{4\pi} \frac{4\pi a^3}{3} \frac{j}{r^3} [3(\hat{j}.\hat{r})\hat{r} - \hat{j}], \tag{4}$$

139 where μ_0 is the magnetic permeability of empty space, j and $\hat{j}$ are the norm and the unit vector of the

140 magnetization vector $(\vec{J} = j.\hat{j})$, and $\hat{r}$ and r are defined as $\overrightarrow{PQ} = \vec{r} = r.\hat{r}$. From equation (3) the

141 magnetic anomaly $C(x, y, z)$ is approximated as the scalar product of $\vec{A}(x, y, z)$ with the unit vector of

142 the regional field $\hat{R}$:

$$C(x, y, z) = \vec{A}(x, y, z) \cdot \hat{R}. \tag{5}$$

143 Equation (4) and (5) show two aspects of the magnetic anomaly illustrated on Figure 2, A and Figure

144 2, B: a magnetic anomaly always has a positive and a negative part and its intensity decreases with

145 $1/r^3$. As a consequence, information on the geometry of the source are lost quickly with an increase

146 in the distance to the source.

147 As $C(x, y, z)$ satisfies Laplace's equation, the spectral frequency w associated with z can be

148 expressed as $w = i\sqrt{u^2 + v^2}$, with u and v the frequencies associated with x and y. This means that

149 it is possible to express the anomaly in the spectral domain through a 2D Fourier transform from a 2D

150 survey and thus facilitate numerical computation as well as simplify several mathematical processes

151 such as deconvolution or derivation[14]. Information on the position, geometry or magnetization of

152 sources can be estimated through potential field transforms such as reduction to the pole,

153 directional derivatives or analytic signel[6].

154 - Reduction to the pole (RTP, Figure 2, C-D) gives the anomaly a symmetrical shape centered on the

155 source and can therefore be used to deduce its horizontal position[15]. It can be written

$$RTP = -\frac{u^2 + v^2}{\left(\alpha_R u + \beta_R v + \gamma_R i\sqrt{u^2 + v^2}\right)\left(\alpha_M u + \beta_M v + \gamma_M i\sqrt{u^2 + v^2}\right)} \tag{6}$$

156 where $(\alpha_R, \beta_R, \gamma_R)$ and $(\alpha_M, \beta_M, \gamma_M)$ are the directional cosines of the regional field and of the

157 magnetization of the source respectively. The direction of the regional field and induced magnetization

158 of the sources is given by IGRF but the direction of remanent magnetization of the sources is usually

159 not known. The application of RTP to locate sources is therefore usually restricted to sources without

160 remanent magnetization.

161 - Directional derivatives in direction $\vec{D}(\alpha, \beta, \gamma)$ can be written

$$\left[-i\left(\alpha u + \beta v + \gamma i\sqrt{u^2 + v^2}\right)\right]^n \tag{7}$$

162 where n is the order of derivative. Significant cases of directional derivatives are the vertical

163 derivative (VD) and the horizontal derivative (HD) that can be expressed from equation (7) as

$$VD = \left(-\sqrt{u^2 + v^2}\right)^n \tag{8}$$

164 and

$$HD = \left(-i\sqrt{u^2 + v^2}\right)^n. \tag{9}$$

165 HD after RTP can be used to locate vertical contacts or vertical limits of a source [16]. VD (Figure 2, G-H)

166 can be used to highlight short wavelengths and thus gain more information on the shape of shallow

167 sources but also enhances noises.

168 - Vector analytic signal is a popular method to lo locate magnetized sources[2]. It is based on the fact

169 that the vertical and horizontal derivatives of the anomaly can be defined as the real and imaginary

170 part of a complex analytic signal[17]. Strictly speaking, only the norm of such an analytic signal is used.

171 In 3D (SA, Figure 2, G-H) it is defined as[18]:

$$|SA| = \sqrt{\left(\frac{\partial C}{\partial x}\right)^2 + \left(\frac{\partial C}{\partial y}\right)^2 + \left(\frac{\partial C}{\partial z}\right)^2}. \tag{10}$$

172 For a perpendicular section of an elongated source, the maximum of SA gives the horizontal position

173 of the source without a priori on its magnetization[17]. For other shapes, the maximum depends on

174 both position and magnetic inclination and none can be accurately deduced[19]. However, if RTP can

175 be applied, the position, depth and magnetic moment of spherical sources can be estimated through

176 an inverse problem[20].

177 As demonstrated, these interpretative methods can be applied on the defined anomaly as it is a

178 potential that satisfies Laplace's equation. In comparison, data obtained with gradiometers are a

179 difference of measurement between two sensors of which the absolute position is not well known.

180 Therefore, the assumption about the difference being a gradient might be inaccurate, especially for

181 ground surveys over shallow sources. In this case the application of interpretative methods cited

182 before might be hazardous and is not recommended. In conclusion, the adapted solution will be

183 different according to the application and budget of the survey.
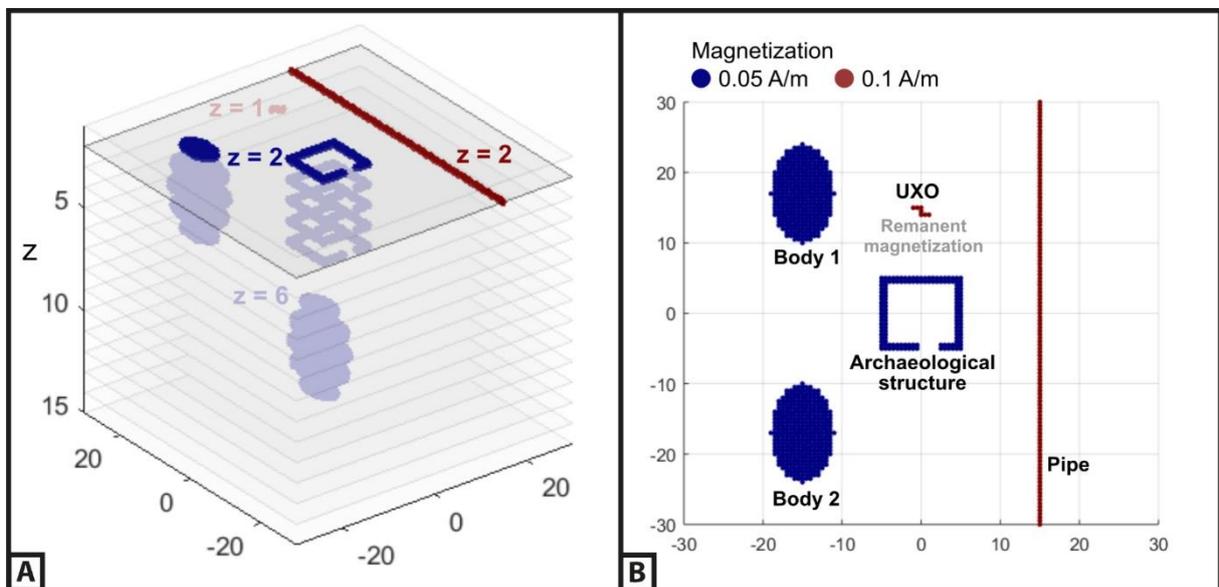
184

185 Figure 1: Synthetic case of buried structures of different shape and magnetization. X and Y axis toward East

186 and North respectively. Z axis corresponds to depth. A - 3D block model. B - Planar overview. Magnetic

187 inclination and declination are set to 40 and 15 degrees respectively for all sources (induced magnetization)

188 except for the UXO for which inclination and declination are set to 60 and -18 degrees to simulate remanent

189 magnetization.
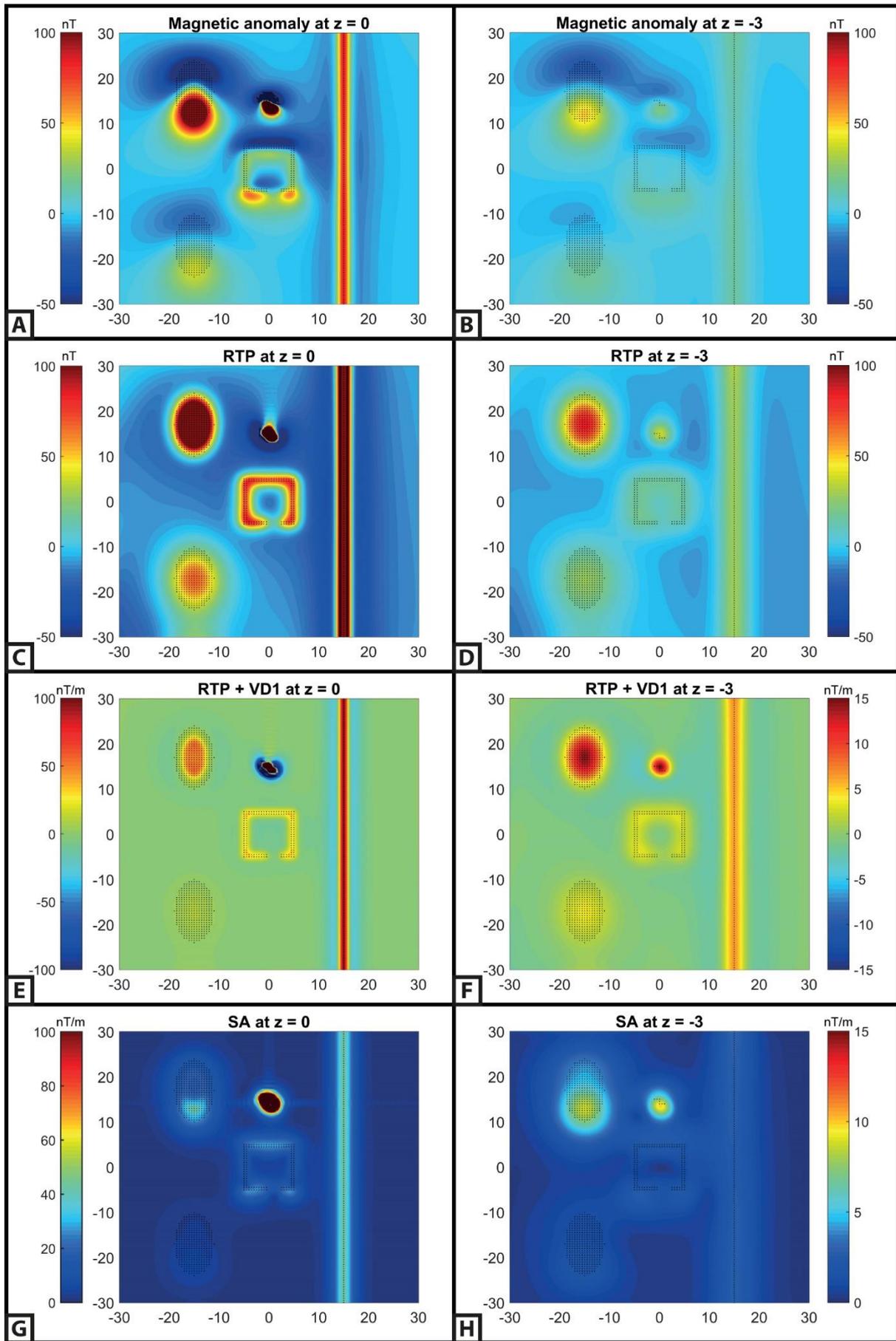
Figure 2: Map of the magnetic anomalies and potential field transforms of the synthetic case presented in

Figure 1. Left column corresponds to a level on the surface (z=0) and the right column to a level at 3 m of

altitude (z = -3). A/B - Magnetic anomaly. C/D - Reduction do the pole (RTP). E/F - First order vertical

derivative (VD1). G/H - Vector analytic signal (SA).

3. How to use Fluxgate three-component magnetometers in applied geophysics

Fluxgate three-component magnetometers are electronic sensors measuring the intensity of the

magnetic field in three orthogonal directions. They are therefore vector magnetometers[21]. They are

light, robust and have a low power consumption. Despite these advantages, they are relative

instruments with inherent errors of offset, sensitivity and angle (non-orthogonality). That is why they

were abandoned for surveying in the 1960's, except for heading correction in AADC systems.

However, Munschy et al[20] showed that such magnetometers can be calibrated and the equipment

mathematically compensated from a simple procedure at the beginning of each survey. This

procedure consists in recording the three components of the magnetic field while moving the whole

system (sensors, digitizer and carrier) in every direction in an area where the magnetic field is known.

On the ground it consists in an area of 1-2 square meters where the device is rotated by 360° around

a fixed point (yaw) while roll movements of +/- 45° are applied. With an airborne carrier the

maneuver consists in flying a clover shape route at a fixed altitude while performing roll movements.

The differences between each three component measurement $F = \left(F_x, F_y, F_z\right)^T$ and the known

magnetic field $B = \left(B_x, B_y, B_z\right)^T$ can thus be associated with noises due to the sensor itself as well as

the magnetizations of the equipment according to the following equation[20]:

$$F = E_O + E_S * E_A * B, \tag{11}$$

where E_O, E_S and E_A correspond to the errors of offset O, sensitivity s and non-orthogonality γ for

each component of the magnetometer such as

$$E_0 = \begin{pmatrix} O_x \\ O_y \\ O_z \end{pmatrix}, \tag{12}$$

$$E_S = \begin{pmatrix} s_x & 0 & 0 \\ 0 & s_y & 0 \\ 0 & 0 & s_z \end{pmatrix}, \tag{13}$$

$$E_A = \begin{pmatrix} 1 & 0 & 0 \\ -\sin\gamma_x & \cos\gamma_x & 0 \\ \sin\gamma_y & \sin\gamma_z & \sqrt{1 - \sin^2\gamma_y - \sin^2\gamma_z} \end{pmatrix}. \tag{14}$$

214   If enough measurements in enough directions are made, i.e. enough different F are measured, the 9

215   parameters O_x, O_y, O_z, s_x, s_y, s_z, γ_x, γ_y, γ_z of the equations (12), (13) and (14) can be estimated

216   through a linearized least-square inverse problem consisting in minimizing by iteration the misfit

217   between measured value and known magnetic field. Once the parameters are estimated, a corrected

218   value F_C of the magnetic field for each measurement F can be calculated as follows:

$$F_C = E_A^{-1} * E_S^{-1} * (F - E_O). \qquad \textbf{(15)}$$

219   Thereby, the intensity of the magnetic field can be computed with a precision suitable for applied

220   geophysics and with higher sampling rates than scalar magnetometer. For example, Institut de

221   Physique du Globe de Strasbourg (IPGS) uses Bartington MAG03 fluxgate three-component

222   magnetometers to survey at sampling frequencies from 25 to 300 Hz, while scalar magnetometers

223   usually have a maximal sampling rate of 10 Hz. For the Bartington MAG03 used by IPGS, the

224   manufacturer gives errors of offset, sensitivity and angle of +/- 5 nT, less than 0.0015 % and less than

225   0.5° respectively, which are typical values for high-end fluxgate magnetometers. This is translated by

226   variations during a calibration and compensation procedure with a standard deviation (STD) of

227   approximately 20 nT. After correction, the STD drops to less than 2 nT[20]. The STD of the corrected

228   values does not depend on the magnetization of the equipment which only affects the STD before

229   correction[22]. However, this result depends on how well the geomagnetic field is known over the area

230   where the compensation procedure is carried out . Usually after correction of the time-dependent

231   variations it can be considered a constant value given either by the IGRF or the median value of the

232   data, but variations of a few nT between the assessed and real values can occur. When the magnetic

233   field is well known, i.e. there is no differences between assessed and real values, STD after correction

234   below 0.5 nT can be obtained[23]. IPGS developed a measuring system which can be mounted on any

235   carrier on the ground or airborne[5]. Its light weight and compensation ability make it especially

236   adapted to be carried by light unmanned aerial vehicles. This opens the range of applications by

237   covering the gap of scale of measurements between ground and airborne surveys. IPGS integrated its

238   system with Bartington MAG03 on different carriers, of which the most commonly used are:

239   - Ground surveys: IPGS uses a multi-sensor device mounted on a backpack using up to eight fluxgate

240   three-component magnetometers placed 0.8 m above the ground to measure simultaneously

241   parallel magnetic profiles with a line spacing of 0.5 m (Figure 3). The compensation ability allows the

242   device to be compact and to integrate additional equipment such as D-GNSS antenna or real time

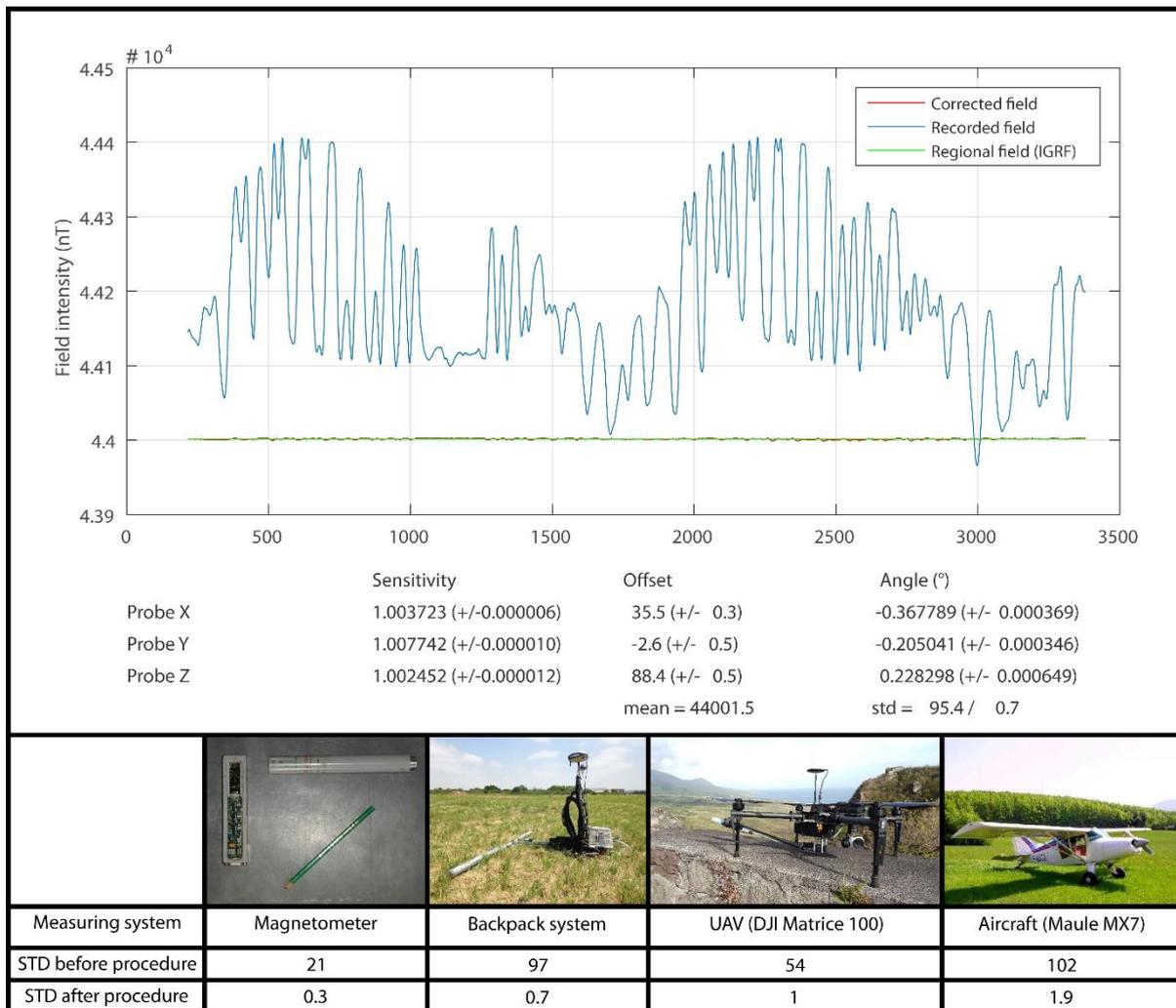243   display of magnetic and navigation data[20,23].

244   - UAV surveys: IPGS uses a mono-sensor device using one fluxgate three-component magnetometer

245   mounted on a light UAV, such as a DJI matrice 100. The magnetometer is slightly shifted from the

246   engines, as they are generating time-dependent variations that as such cannot be compensated. The

247   calibration and magnetic compensation of the rest of the equipment (UAV, GNSS antenna) is

248   completed through a maneuver where the UAV performs roll and yaw over an area of a few square

249   meters at a fixed elevation (usually 50 m), in a way similar to the procedure for ground devices. The

250   UAV can acquire data at speed ranging from 3 to 60 km/h, at elevation between 1 and 200 m above

251   the ground, either draping the topography or at a fixed level. Distance to ground is either planned

252   beforehand from a numerical model or assessed in real time with a laser depending on the

253   availability and resolution of an elevation model of the area as well as the risk of unplanned obstacles

254   such as vehicles or vegetation for surveys carried at very low elevation (usually less than 30 m).

255   - Airborne surveys: IPGS uses a mono-sensor device mounted on a simple aircraft[22], a gyrocopter[24] or

256   ultra-light aircraft[5]. The calibration and compensation procedure is carried out through a clover

257   shaped figure.

258   Figure 3 shows uncorrected and corrected measurements obtained through the typical calibration

259   and compensation procedure explained above as well as the average STD before and after correction

260   for a single magnetometer and different carriers (ground, UAV, airborne). The differences of STD

261   after corrections between carriers are mainly explained by unknown variations of the magnetic field

262   in the area of the procedure but could also indicate uncorrected time-dependent variations (such as

263   electromagnetic fields from the battery or engine) or a difference of the number of visited attitudes

264   during the procedure which are usually lower with airborne carrier than on the ground. Regardless of

265   the carrier, the STD after correction is always lower than 2 nT.

266

The figure contains a chart with axes labeled "Field intensity (nT)" (y-axis) and values 4.39 to 4.45 (×10⁴), x-axis from 0 to 3500. Legend: Corrected field (red), Recorded field (blue), Regional field (IGRF) (green).

Below the chart:

	Sensitivity	Offset	Angle (°)
Probe X	1.003723 (+/-0.000006)	35.5 (+/- 0.3)	-0.367789 (+/- 0.000369)
Probe Y	1.007742 (+/-0.000010)	-2.6 (+/- 0.5)	-0.205041 (+/- 0.000346)
Probe Z	1.002452 (+/-0.000012)	88.4 (+/- 0.5)	0.228298 (+/- 0.000649)
		mean = 44001.5	std = 95.4 / 0.7

Measuring system	Magnetometer	Backpack system	UAV (DJI Matrice 100)	Aircraft (Maule MX7)
STD before procedure	21	97	54	102
STD after procedure	0.3	0.7	1	1.9

Figure 3: Intensity of the magnetic field measured by one fluxgate three_component magnetometer (Bartington MAG03) during the calibration and compensation process of the backpack mounted device. The raw data is shown in blue, corrected data in red and regional field in green. Applied correction parameters (sensitivity, offset and angle) for each probe of the sensor are shown below the curves. The table shows the standard deviation before and after the corrections of the calibration and compensation procedure for different carriers.

## 4. Case study

In order to assess the possibilities offered by the use of fluxgate three-component magnetometers, a few examples of application at different scales and with different carriers are presented. Case studies 1 and 4 are partially published in Gavazzi et al.23 and Munschy and Fleury22 respectively while 2 and 3 are unpublished work form IPGS.

4.1 On the ground: high resolution for archaeological applications

During the study of the site of Qasr 'Allam in the oasis of Bahariya in the Western desert of Egypt, an area was surveyed by two measuring system, as reported by Gavazzi et al.[23]: the backpack mounted system (Figure 3) in the framework of a collaboration between archaeologists and IPGS, and a

283 vertical component gradiometer very common in archaeological and other near-surface applications

284 (Geoscan FM 256) in the framework of a commercial service conducted by a team of the Institute of

285 Archaeology and Ethnology of the Polish Academy of Sciences. The two devices measure different

286 physical quantities: the vertical component gradient for the gradiometer and the total magnetic field

287 intensity for the backpack system. However, gradient and intensity can be calculated from one

288 another using potential field theory: gradient is a derivative of intensity and therefore intensity an

289 integral of gradient, both easily calculated in the spectral domain after a gridding step. Thus

290 calculated and measured quantities for each dataset can be compared and should be similar.

291 Gridding is done with a 0.25 m step and the measured and calculated anomaly of the total magnetic

292 field and vertical component gradient are shown in Figure 4. The two maps of vertical gradient are

293 mostly similar as expected, the slight differences being due to different level of imprecision for the

294 two surveys as well as slight differences in distance to the ground of the sensors. The two maps of

295 the anomalies of the total magnetic field show strong differences: large wavelength anomalies

296 appear on the map calculated from the measured gradient compared to the measured anomalies.

297 This cannot be due to edge effects which should be following the direction of the axes x and/or y.

298 The differences are mainly due to imprecisions in the measurements that are enhanced through the

299 calculation process. Indeed, the fact that the two sensors of a gradiometer cannot be maintained

300 exactly vertical during the survey leads to imprecisions small enough to be considered not significant

301 when the gradient is directly displayed but important enough to pose problem in potential field

302 calculations. Thus Figure 4 illustrates why using interpretative methods from potential field theory on

303 gradiometers data can be hazardous and is not recommended. In the case of the study, most of the

304 anomalies have short wavelengths and can be interpreted on both surveys as irrigation channels

305 while anomalies with large wavelengths, corresponding to deeper sources such as older channels and

306 wells can only be interpreted on the results of the backpack system. Another difference between the

307 two systems is the surveying time for the same area: approximately two days for the survey with a

308 single gradiometer and one hour for the survey with the backpack system. The greater speed of the

309 backpack system is due to its multi-sensors aspect as well as the integration of real time positioning

310 using a GNSS system. Thus the system allows to acquire four simultaneous profiles with no

311 preparations on the field while the gradiometer allows to measure only one profile at a time and

312 requires the set-up of a georeferenced grid on the field. Such step can take more time than the

313 recording itself.
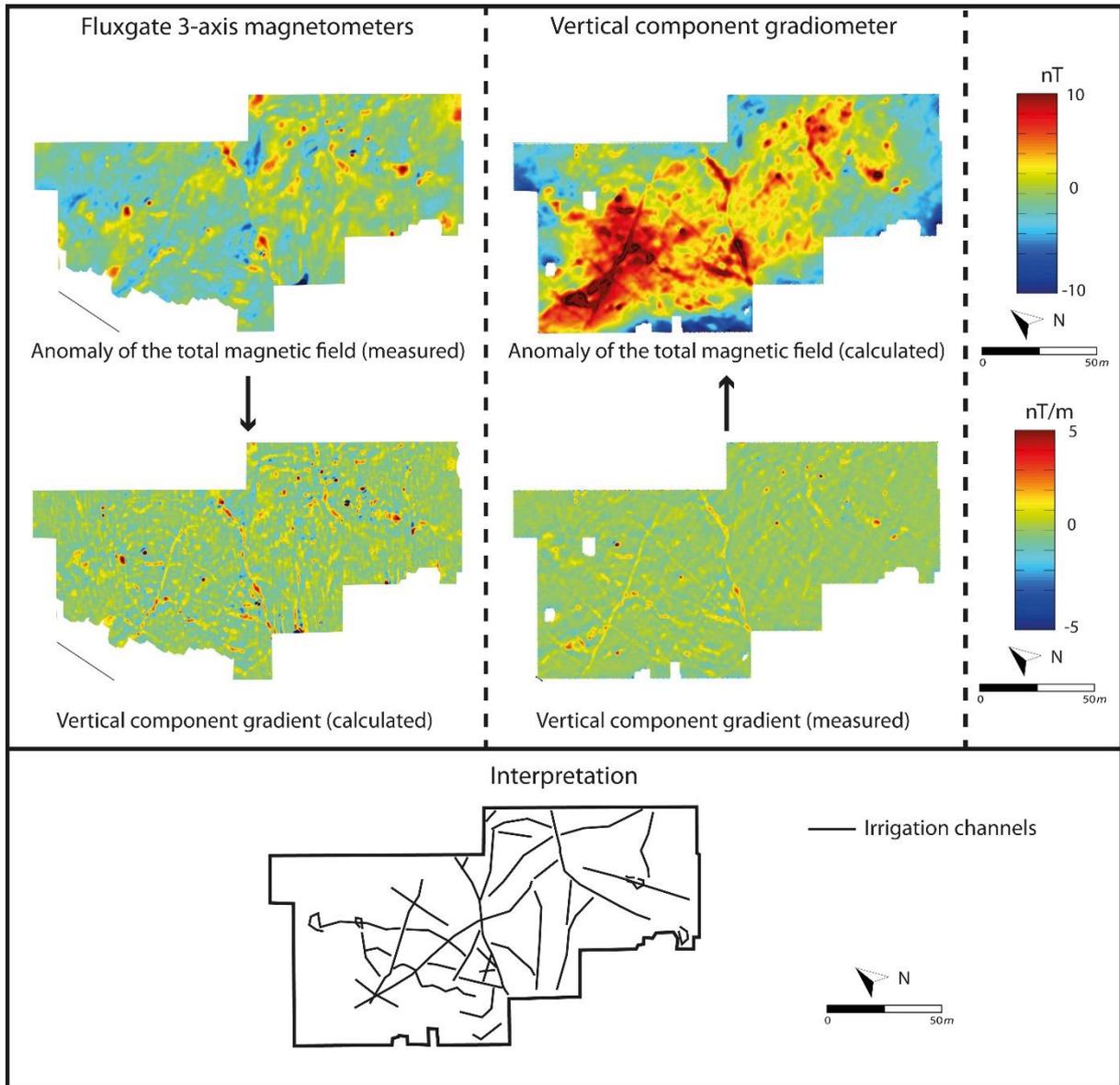
Figure 4: Comparison of two surveys of the same area with different devices and resulting interpretation. Anomaly of the total magnetic field and vertical component gradient are either measured or computed according to the surveying device.

4.2 UAV-borne and ground surveys for the detection of Unexploded Ordnance

The former French army aerial base BA112 contains many residues of the two last world wars: unexploded ordnance (UXO), ammunition stocks, trenches, tunnels... In the framework of a collaboration between CARDEM and IPGS an area was surveyed with different devices using fluxgate three-component magnetometers to assess the anthropogenic pollution of the underground as well as to compare the limit of detection of different carriers. A ground survey at 0.8 m above the ground was conducted with a backpack system as well as an UAV survey 3 m above ground level with a greater speed but lower resolution than the ground survey. Figure 5-A presents the observed maps of the magnetic anomaly for the two surveys and the corresponding maps of the vector analytic

327 signal to assess the horizontal position of the sources. As the distance of sensors to the ground

328 increases, the wavelengths of the anomalies increase and their amplitudes decrease. The orange,

329 blue and green lines on the interpretative map in Figure 5-B show different patterns of anomalies.

330 The orange lines highlight the presence of buried networks or pipes, the green line highlights a part

331 of a trench from the first world war and the blue lines highlight the remains of an old building. All

332 dipole anomalies might correspond to UXO as well as other concentrated metallic material. Depth

333 and magnetization of these potential UXO are evaluated from each dataset through an inverse

334 problem on the analytic signal, assuming a spherical geometry (i.e. that the UXO are compact) and

335 after a reduction to the pole assuming only induced magnetization. This assumption is common in

336 UXO detection due to a great reduction of the remanent magnetization by the shock of firing and

337 impact[25]. Three anomalies are selected to illustrate the limits of the method:

338 - Source A: the digging revealed a piece of wire mesh at a depth of 0.54 m, similar to the estimated

339 depth from the two dataset (0.5 and 0.7 m, the difference is explained by the lower accuracy level of

340 the GNSS antenna mounted on the UAV than on the backpack). The estimated magnetization from

341 the UAV survey (44.5 A.m^2) is twice the one from the backpack survey (18.2 A.m^2).

342 - Source B: the digging revealed three screw pickets at a depth of 0.68 m, similar to the depth given

343 from the backpack survey (0.7 m). The UAV survey gives an overestimated depth (1.1 m), probably

344 due to the lower accuracy of the GNSS antenna. The estimated magnetization from the backpack

345 survey (74.2 A.m^2) is twice the one from the UAV survey (42 A.m^2).

346 - Source C: the digging revealed 14 screw pickets, barbed wire and shrapnel at a depth of 1.28 m,

347 which differs greatly from the depth given from the backpack survey (2.5 m) and UAV survey (0 m).

348 The estimated magnetization from the backpack survey (4738 A.m^2) is five times the one from the

349 UAV survey (884 A.m^2).

350 The differences in depth and magnetization estimations can be due to the non-spherical geometry of

351 the sources. Indeed, depth estimations for sources A and B which consist in 1 and 3 objects are

352 consistent with field evidences while the estimations for source C which consists in 14 objects are not

353 consistent and differ with the field evidence. A similar effect seems to impact the estimation of

354 magnetization but with a greater extent, as none of the estimated values are consistent. A presence

355 of remanent magnetization could also play a role in these inaccuracies. In conclusion, both surveys

356 seem to provide a good lateral position of the different sources but depth and magnetization

357 estimations should be used cautiously as they can lead to significant errors if the sources are not a

358 compact enough or composed of several objects.

359
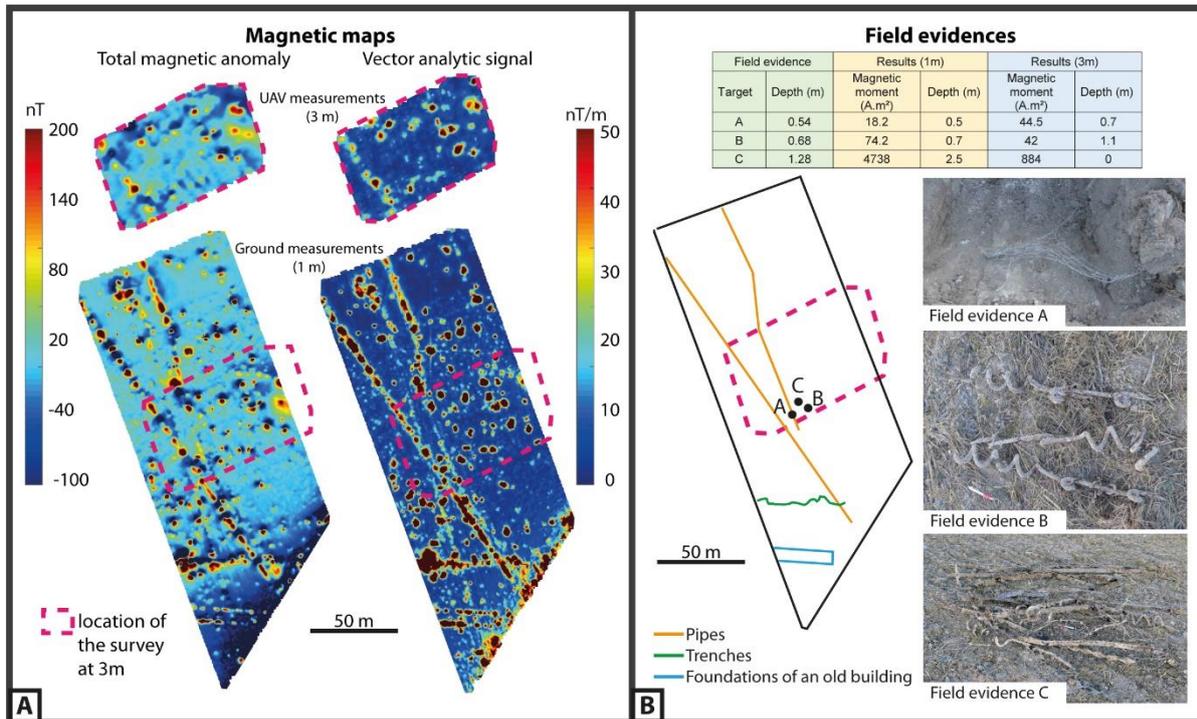
Figure 5: A - Maps of the magnetic anomalies to the left and maps of the vector analytic signal to the right for the two surveys (UAV and Backpack). B - Interpretative map of significant structures (trenches, pipes and old building) and comparison of interpretation and field evidence obtained for dipole anomalies A, B and C.

4.3 UAV-borne surveys for high resolution lithological and structural studies

A magnetic cartography using a light UAV was performed by IPGS in collaboration with Teranov in the framework of St kitts geothermal project. The goal of the survey is to improve the geological structural interpretation of a part of the island. Because of the dense vegetation and steep topography (slope angles reach more than 35°), ground measurements are almost impossible. Airborne magnetic measurements are also ruled out for the same reason: an airplane cannot follow such a topography at a low altitude.

A light UAV (DJI Matrice 100) equipped by IPGS with a Bartigton fluxgate three-component magnetometer was used to produce a draping magnetic map 100 m above ground, with a line-spacing of 100 m and for a total area of 13 km². From June 27th to July 1st 2016, the UAV has flown 218 km distributed in 107 km of profiles, 30 km of tie-lines and 81 km for transit (Figure 6, A). The resulting dataset was used to compute the total magnetic intensity. The anomaly of the magnetic intensity map presented in figure 6, A is computed by removing the regional field given by the IGRF from the data after correction of the time-dependent variations. This first map shows SW-NE directions consistent with the local fault network[26,27] and a circular anomaly correlated to the Brimstone hill andesitic dome[28,29].

381   One major direction near Brimstone hill was identified as an area of interest. To better understand

382   the magnetic anomalies in this specific zone, a 25 m above ground draping survey was conducted.

383   This survey was flown with a 25 m line-spacing between the 2nd and the 5th of July 2016 for a total of

384   28 km of magnetic profiles and tie-lines and an area of 0.65 km². The resulting anomaly map is

385   overlaid on the previous 100 m survey on Figure 6, B.

386   The contribution of the 25 m survey is better seen on Figures 6, C and 6, D presenting the reduction

387   to the pole of the magnetic anomaly in the area of interest. The large SW-NE direction previously

388   identified is revealed to be constituted of two smaller and discontinued lineaments as shown in

389   figure 6, E and 6, F. The discontinuity of these anomalies indicates the presence of a structural

390   direction N020 that was not previously recognized in this area.

Figure 6: Saint Kitts UAV surveys. Left column: 100 m above the ground survey, Right column: superposition of 100 m and 25 m above the ground surveys, zoomed in the red squares. A/B - Maps of the anomalies of the total magnetic intensity. C/D/E/F - Maps of the reduction to the pole of the anomalies. Color scales are kept consistent for all surveys and representations.

4.4 Airborne surveys for large scale lithological and structural studies and comparison with industrial standard

In the framework of a geothermal exploration project, two surveys were conducted in the Vosges mountain with different measuring systems. A first survey at a fixed level of 1000 m above sea level was conducted in 2008 by IPGS with its own measuring system using one Bartington fluxgate three-component magnetometer mounted on a Maule MX7. The second survey took place in 2015 and was executed by the geophysics contractor *eGeophysics GPR international Inc.* with an absolute Geometrics cesium magnetometer mounted on a custom helicopter Ecureuil AS350 and a RMS Instruments AADC for real time compensation. This survey draped the topography at 300 m above ground level and the altitude of the data is varying between 400 and 1400 m above sea level. Both surveys are overlapping in an area of roughly 20 x 10 km but at different altitudes. In order to compare both datasets an upward continuation to the level of the highest data point (1400 m) is calculated. The resulting maps are shown in Figure 7. The different anomalies correspond to structural features or lithological contacts that will be discussed with geologists. In the overlapping area, no differences are visible between the results of the two different devices, thus illustrating a similar level of quality of data between a system using a fluxgate three-component magnetometer and an industrial system using a cesium magnetometer. The main difference lies in the cost: the system used by IPGS costs around 5 k€ while scalar magnetometers have a higher price range (15 k - 50 k€) and require the addition of an AADC (100k - 200 k€) for the magnetic compensation of the carrier. Thus, for a same carrier, the difference of price between the two types of measuring systems is of a factor ranging between 20 and 50.

417
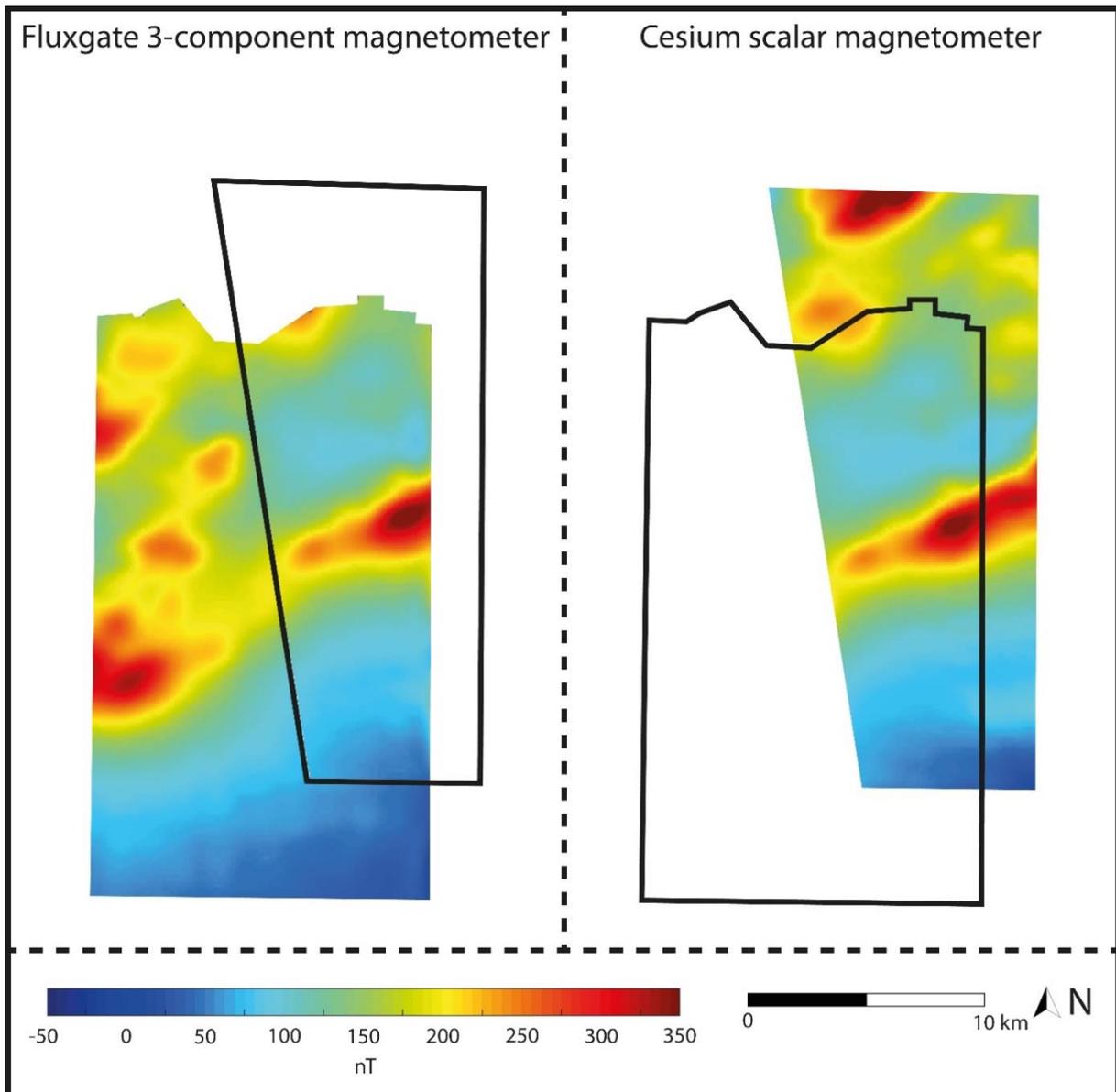
Figure 7: Comparison of results of magnetic surveys over the same area in the Vosges mountains with two different systems: Left - survey conducted in 2008 by IPGS with a Maule MX7 with Bartington MAG03 fluxgate three-component magnetometers; right - survey conducted in 2015 by Geophysics GPR International Inc. with a AS 350 Ecureuil with Geometrics Cesium scalar magnetometer and a RMS instruments compensation system.

5. Conclusion

As illustrated by the different examples, measuring systems using fluxgate three-component magnetometers can be a good alternatives to different standards in use in applied geophysics. In airborne surveys, they provide results with the same quality and precision than industrial systems based on scalar magnetometers at a fraction of their cost (20 to 50 times less). In ground surveys, they are often faster than other devices and the results are less prone to noise than gradiometer results when interpretative potential field transformations are used. In addition, they can be

430   mounted on light UAVs and aircrafts, filling the scale gap between detailed ground surveys and

431   regional airborne surveys. This ability to survey at any scales offers new resolution of data and thus

432   new possibilities of application. The system developed by IPGS is currently used for archaeology, UXO

433   detection, pipe detection and resources exploration but could be used in any application where

434   heterogeneities within the ground must be assessed.

5. Acknowledgement

Bibliography

445   1. Reynolds JM. *An introduction to applied and environmental geophysics*. John Wiley & Sons; 1997.

446   2. Nabighian MN, Grauch VJS, Hansen RO, et al. The historical development of the magnetic method

447   in exploration. *Geophysics*. 2005; 70(6): 33ND–61ND. doi: 10.1190/1.2133784

448   3. Linford N. 2006. The application of geophysical methods to archaeological prospection. *Rep on

449   Prog in Phys*. 2006. 69: 2205-2257. doi: 10.1088/0034-4885/69/7/R04

450   4. Liu Q, Roberts AP, Larrasoaña JC, et al. Environmental Magnetism: principles and applications. *Rev

451   of Geophys*. 2012; 50(4): RG4002. doi: 10.1029/2012RG000393

452   5. Gavazzi B, Le Maire P, Munschy M, Dechamp A. Fluxgate vector magnetometers: A multisensor

453   device for ground, UAV, and airborne magnetic surveys. *The Lead Edge.* 2016; 35(9): 795-797. doi:

454   10.1190/tle35090795.1

455   6. Blakely RJ. *Potential Theory in Gravity & Magnetic Applications*. Cambridge University Press; 1995.

456   7. Telford W, Geldart L, Sheriff R. *Applied Geophysics*. Cambridge University Press; 1990. doi:

457   10.1017/CBO9781139167932

458   8. Thébault E, Finlay CC, Begga CD, Alken P, Aubert J, Barrois O, Bertrand F, Bondar T, Boness A,

459   Brocco L, Canet E, Chambodut A, Chulliat A, Coïsson P, Civet F, Du A, Fournier A, Fratter I, Gillet N,

460   Hamilton B, Hamoudi M, Hulot G, Jager T, Korte M, Kuang W, Lalanne X, Langlais B, Léger JM, Lesur V,

Lowes FJ, Macmillan S, Mandea M, Manok C, Maus S, Olsen N, Petrov V, Ridley V, Rother M, Sabaka TJ, Saturnino D, Schachtschneider R, Sirol O, Tangborn A, Thomson A, Tøffner-Clausen L, Vigneron P, Wardinski I, Zvereva T. International Geomagnetic Reference Field: the 12th generation. *Earth, Planets and Space.* 2015. 67:79. doi: 10.1186/s40623-015-0228-9

9. Horsfall KR. Airborne magnetic and gamma-ray data acquisition. *AGSO J of Aust Geol & Geophys.* 1997; 17(2): 23-30

10. Coyle M, Dumont R, Keating P, Kiss F, Miles W. Geological Survey of Canada aeromagnetic surveys: design, quality assurance, and data dissemination. *Geological survey of Canada*, open file 7660. doi: 10.4095/295088

11. Butler DK. Implications of magnetic backgrounds for unexploded ordnance detection. *J of Appl Geophys*. 2003; 54 (1-2): 111-125. doi: 10.1016/j.jappgeo.2003.08.022

12. Gaffney C. Detecting trends in the prediction of the buried past: A review of geophysical techniques in archaeology. *Archaeom*. 2008; 50: 313–336. doi: 10.1111/j.1475-4754.2008.00388.x

13. Zalevsky Z, Bregman Y, Salomonski N, Zafrir H. Resolution Enhanced Magnetic Sensing System for Wide Coverage Real Time UXU Detection. *J of Appl Geophys.* 2012; 84: 70-76. doi: 10.1016/j.jappgeo.2012.06.003

14. Bhattacharyya BK, Navolio ME. A fast fourier transform method for rapid computation of gravity and magnetic anomalies due to arbitrary bodies. *Geophysic Prospect.* 1976; 24: 633-649. doi: 10.1111/j.1365-2478.1976.tb01562.x

15. Baranov V. 1957. A new method for interpretation of aeromagnetic maps: pseudo gravimetric anomalies. *Geophys*. 1957; 22: 359-383. doi: 10.1190/1.1438369

16. Grauch VJS, Cordell L. Limitations of determining density or magnetic boundaries from the horizontal gradient of gravity or pseudogravity data. *Geophys*. 1987; 52(1): 118–121. doi: 10.1190/1.1442236

17. Nabighian MN. The Analytic Signal of Two-Dimensional Magnetic Bodies with Polygonal Cross-Section; Its Properties and Use for Automated Anomaly Interpretation. *Geophys.* 1972; 37(3): 507-517. doi: 10.1190/1.1440276

18. Roest WR, Verhoef J, Pilkington M. Magnetic Interpretation Using the 3-D Analytic Signal. *Geophys.* 1992*;* 57(1): 116-25. Doi: 10.1190/1.1443174

490 19. Salem A, Ravat D, Gamey TJ, Ushijima K. Analytic signal approach and its applicability in

491 environmental magnetic investigations. *J of Appl Geophys*. 2002; 49(4): 231–244. doi:

492 10.1016/S0926-9851(02)00125-8

493 20. Munschy M, Boulanger D, Ulrich P, Bouiflane M. Magnetic mapping for the detection and

494 characterization of UXO: Use of multi-sensor fluxgate 3-axis magnetometers and methods of

495 interpretation. *J of Appl Geophys*. 2007; 61: 168-183. doi: 10.1016/j.jappgeo.2006.06.004

496 21. Primdahl F. The fluxgate magnetometer. *J of Phys E: Sci Instrum*. 1979; 12(4): 241-253. doi:

497 10.1088/0022-3735/12/4/001

498 22. Munschy M, Fleury S. Scalar, vector, tensor magnetic anomalies: measurement or computation?

499 *Geophys Prospect*. 2011; 59: 1035-1045. doi: 10.1111/j.1365-2478.2011.01007.x

500 23. Gavazzi B, Alkhatib-Alkontar R, Munschy M, Colin F, Duvette C. On the Use of Fluxgate 3-Axis

501 Magnetometers in Archaeology: Application with a Multi-sensor Device on the Site of Qasr 'Allam in

502 the Western Desert of Egypt. *Archaeol Prospect*. 2017; 24(1): 59-73. doi: 10.1002/arp.1553

503 24. Ameglio L, Jacobs G, Von Ludwig J, Munschy M. GyroLAG - fluxgate magnetic total field, vectors,

504 and tensors mapping. *The Lead Edge.* 2011; 30(6): 674-680. doi: 10.1190/1.3599154

505 25. Billings S, Beran L. Experimental measurements of shock induced changes to the magnetization of

506 unexploded ordnance. *J of Appl Geophys.* 2014; 105: 138-146. doi: 10.1016/j.jappgeo.2014.03.015

507 26. Feuillet N, Leclerc F, Tapponnier P, et al. Active faulting induced by slip partitioning in Montserrat

508 and link with volcanic activity: New insights from the 2009 GWADASEIS marine cruise data. *Geophys

509 Res Lett*. 2010; 37(19): L00E15. doi: 10.1029/2010GL042556

510 27. Feuillet N, Beauducel F, Tapponnier P. Tectonic context of moderate to large historical

511 earthquakes in the Lesser Antilles and mechanical coupling with volcanoes. *J of Geophys Res: Solid

512 Earth*. 2011; 116: B10308. doi: 10.1029/2011JB008443

513 28. Baker PE. The geological history of Mt Misery Volcano, St Kitts, West Indies. *Overseas Geol and

514 Miner Resour*. 1969; 10(3): 207-230. doi: 10.1016/S0024-4937(68)80004-0

515 29. Roobol MJ, Smith AL. *Geological map of St. Kitts, West Indies;* 2015